Organic & Biomolecular Chemistry

Accepted Manuscript

ROYAL SOCIETY OF CHEMISTRY

www.rsc.org/obc

Cite this: DOI: 10.1039/c0xx00000x

www.rsc.org/xxxxxx

ARTICLE TYPE

Luminescent organogels based on triphenylamine functionalized β-diketones and their difluoroboron complexes

Chong Qian, Mingyang Liu, Guanghui Hong, Pengchong Xue, Peng Gong and Ran Lu*

Received (in XXX, XXX) Xth XXXXXXXXX 20XX, Accepted Xth XXXXXXXXX 20XX

DOI: 10.1039/b000000x

A series of new triphenylamine functionalized β-diketones **1**-**3** and their difluoroboron complexes **1B**-**3B** were synthesized. They exhibited strong intramolecular charge transfer (ICT) emission. It was found that their self-assembling properties depended on the molecular structures. For example, compounds **1** and **1B**, in which only one β-diketone or difluoroboron β-diketone unit linked to triphenylamine, showed better gelation abilities directed by π-π interaction. Although bis-β-diketone substituted triphenylamine **2** could not form organogel, its difluoroboron complex **2B** could gel DMSO due to the strong dipole-dipole interactions. Compound **3** could form gels in polar solvents, while **3B** formed gels in nonpolar solvents. Notably, the asymmetric gelators **1**, **1B** and **2B** exhibited AIEE behaviors during the gelation. Although the emission of the symmetric compounds **3** and **3B** decreased to a certain degree upon gelation, the obtained gels still gave strong emission. The gels formed from **1** and **3** emitted strong green light and those based on **1B**-**3B** emitted strong orange or red light. These highly luminescent materials might have potential applications in emitting devices and fluorescent sensors.

Introduction

Over the past decades, low molecular weight organogels (LMOGs), as an important class of soft materials, have attracted substantial interest in supramolecular chemistry and material science because of their diverse applications in the fields of lubrication industry, cosmetic formulations, template synthesis, regenerative medicine, tissue engineering, self-healing materials and so on.[1] In particular, LMOGs based on π-conjugated organic compounds have currently received even more attention for their unique optoelectronic applications in multicolor display devices, light harvesting antennae, field effect transistors, photovoltaic devices, conducting materials, fluorescence sensors, etc.[2] So far, a variety of π-gels containing the chromophores of oligo(phenylenevinylene)s,[3] perylene bisimides,[4] trifluoromethyl aromatics,[5] pyrene[6] and carbazoles[7] have been developed. However, it is still a challenge to construct new π-gels with enhanced performance in optoelectronic devices.

It has been known that β-diketones usually existed in a hydrogen-bonded six-membered ring via tautomerization between ketone and enol forms, which can increase the molecular planarity and lead to the inhibition of the nonradioactive dissipation. Moreover, β-diketone can chelate with many kinds of cations, including metal ions (rare earth, zinc, aluminium ions, etc) and boron ion to yield the complexes with high emission.[8] For example, Tian et al. have prepared bis-β-diketonate phenothiazine ligands and the corresponding cyclic dinuclear complexes, in which Zn(II) complexes are better candidates for two-photon microscopy images of living cells.[8d] Cheng and coworkers have synthesized new platinum phosphors containing an aryl-modified β-diketonate ligands, and the non-doped electroluminescence device using platinum phosphors as the emitter gives an external quantum efficiency of 10%.[8e] In particular, on account of high quantum yields, large molar extinction coefficients, strong emission in solid state, high electron affinities and sensitivity to the surrounding medium,[9] difluoroboron β-diketonate complexes have been employed in nonlinear optical materials,[10] mechanochromic luminescent materials,[11] near-IR probes,[12] solar cells[13] and organic field-effect transistors.[14] However, to the best of our knowledge, there are only few reports on the construction of LMOGs based on difluoroboron β-diketonate complexes. For instance, Maeda et al. synthesized boron complexes of aryl-substituted dipyrrolyldiketones derivatives and investigated the anion-responsive behaviors in gel state.[15] Our group has generated the emissive nanofibers based on difluoroboron β-diketone complexes via organgelation, which could sense gaseous organic amines with high sensitivity and fast response.[7d,16] Thus, we envisioned that β-diketone and their difluoroboron complexes could serve as unique platform for the construction of new luminescent organogels. We have found that the terminal triphenylamine linked to difluoroboron β-diketone complexes was favorable for the gel formation directed by balanced π-π interaction. Herein, we employed triphenylamine as the core to link with different numbers of β-diketone units in order to reveal the relationship between molecular structures and gelation properties. New β-diketone ligands **1**-**3** and their difluoroboron complexes **1B**-**3B** were designed (Scheme 1). It was found that the synthesized compounds except **2** could form stable gels in tested solvents. Interestingly, the compounds **1**, **2** and **2B** with

asymmetric structures exhibited aggregation-induced enhanced emission (AIEE) during the gelation processes, while the emission of the symmetric compounds **3** and **3B** decreased upon gelation. Meanwhile, in the gels as well as in the xerogel films, β-diketones **1** and **3** emitted strong green light and difluoroboron β-diketonate complexes **1B**-**3B** emitted strong orange or red light. Therefore, we provide a strategy to design new organogelators based on β-diketones and difluoroboron β-diketonate complexes with AIEE during gelation, which would be employed as emitters in OLEDs, sensors or related fields.

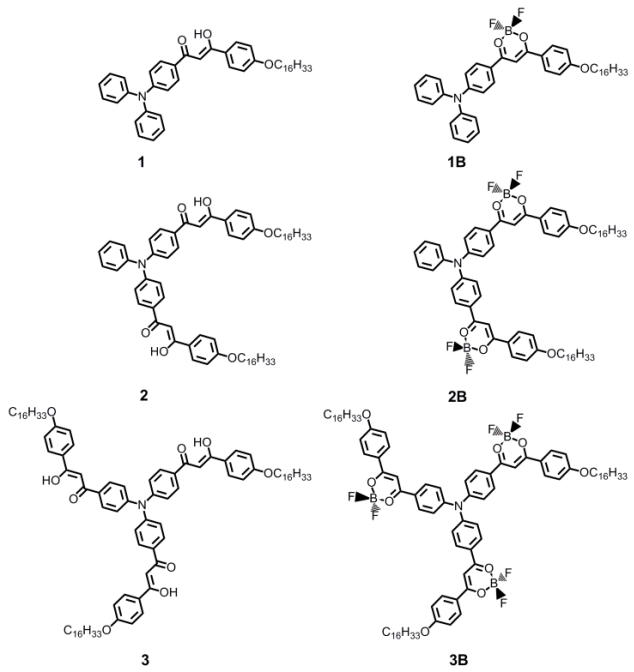

Scheme 1 Molecular structures of β-diketones **1**-**3** and their difluoroboron complexes **1B**-**3B**.

Experimental section

Measurements and characterizations

^{1}H NMR spectra were recorded on a Bruker Avance III 500 MHz and 400 MHz using $CDCl_3$ as solvents. ^{13}C NMR spectra were recorded on Bruker Avance III 125 MHz and 100 MHz using $CDCl_3$ as solvents. Mass spectra were performed on Agilent 1100 MS series and AXIMA CFR MALDI/ TOF (matrix assisted laser desorption ionization/time-of-flight) MS (COMPACT). IR spectra were measured with a Nicolet-360 FT-IR spectrometer by incorporation of samples in KBr disks. C, H, and N analyses were taken on a Vario EL cube elemental analyzer. UV-vis absorption spectra were determined on a Shimadzu UV-1601PC spectrophotometer. Fluorescence emission spectra were carried out on a Shimadzu RF-5301 luminescence spectrometer. The fluorescence quantum yields of the samples in solid state were measured by an Edinburgh Instrument FLS920 using an integrating sphere. Scanning electron microscopy (SEM) images was obtained on a JEOL JSM-6700F and HITACHI SU8020. The samples for SEM measurement were prepared by casting the organogels on silicon wafers and dried in vacuum oven at room temperature, followed by coated with gold. Fluorescence microscopy images were taken on Fluorescence Microscope (Olympus Reflected Fluorescence System BX51, Olympus, Japan). X-ray diffraction patterns were obtained on a PANalytical B.V. Empyrean or Rigaku Smartlab. XRD equipped with graphite monochromatized Cu Kα radiation (λ =1.5418 Å), employing a scanning rate of 2° min^{-1} in the 2θ range from 1° to 30°. The samples for fluorescence microscopy and XRD measurements were prepared by casting the gels on glass slide and dried in vacuum oven at room temperature.

Computational methods

All compounds were modeled using the Gaussian 09 suite of programs using density functional theory. The groud-state geometries of six compounds with hexadecyl were optimized by B3LYP/6-31G method. We used time-dependent density functional theory, TD-B3LYP/6-31G for estimate of the absorption spectra, at the respective optimized geometries without the solvent correction. Hexadecyl in compound **2** and **3B** were replaced by methyl in TD-DFT calculation. Other compounds were calculated with hexadecyl. Molecular orbitals and computed absorption spectra were depicted by GaussView 5.0 software.

Materials and synthesis

THF was freshly distilled from sodium and benzophenone under nitrogen. CH_2Cl_2 was distilled from CaH_2. All the other chemicals and reagents were used as received from commercial sources without further purification. Compounds **4**, **5**, **6**[17] (Scheme 2)

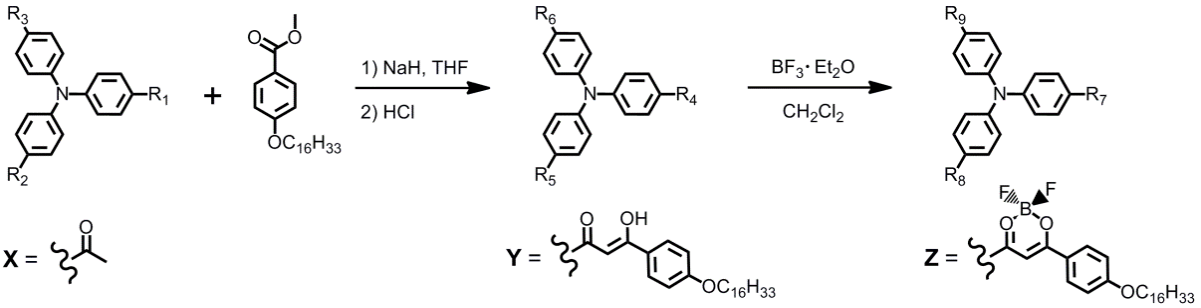

4: R_1 = **X**, R_2 = R_3 = H
5: R_1 = R_2 = **X**, R_3 = H
6: R_1 = R_2 = R_3 = **X**

1: R_4 = **Y**, R_5 = R_6 = H
2: R_4 = R_5 = **Y**, R_6 = H
3: R_4 = R_5 = R_6 = **Y**

1B: R_7 = **Z**, R_8 = R_9 = H
2B: R_7 = R_8 = **Z**, R_9 = H
3B: R_7 = R_8 = R_9 = **Z**

Scheme 2 Synthetic routes for β-diketones **1**-**3** and their difluoroboron complexes **1B**-**3B**.

Cite this: DOI: 10.1039/c0xx00000x

www.rsc.org/xxxxxx

ARTICLE TYPE

and methyl 4-(hexadecyloxy)benzoate[18] were synthesized according to the literatures.

(Z)-1-(4-(diphenylamino)phenyl)-3-(4-(hexadecyloxy)phenyl)-3-hydroxyprop-2-en-1-one (1).

Sodium hydride (60%, 0.28 g, 6.96 mmol) was added quickly to a dry flask containing a solution of compound **4** (1.00 g, 3.48 mmol) and methyl 4-(hexadecyloxy)benzoate (1.57 g, 4.18 mmol) in THF (30 mL). The reaction mixture was refluxed under an atmosphere of nitrogen for 24 h. The solution was cooled to the room temperature and then acidified with dilute HCl. The mixture was poured into water and extracted with dichloromethane for three times. Then the organic phase was combined and dried over anhydrous Na_2SO_4. Removing the solvent under reduced press, the residue was purified by column chromatography (silica gel, CH_2Cl_2/petroleum ether, v/v = 1/1), followed by recrystallization from ethanol to afford compound **1** (1.1 g) as a yellow solid. Yield: 49%. mp: 66.0-68.0 °C. ^{1}H NMR (400 MHz, $CDCl_3$): δ 17.12 (s, 1H), 7.93 (d, *J* = 8.8 Hz, 2H), 7.82 (d, *J* = 8.8Hz, 2H), 7.32 (t, *J* = 8.0 Hz, *J* = 8.0 Hz, 4H), 7.17-7.11 (m, 6H), 7.04 (d, *J* = 8.8 Hz, 2H), 6.95 (d, *J* = 8.8 Hz, 2H), 6.70 (s, 1H), 4.02 (t, *J* = 6.8 Hz, *J* = 6.4 Hz, 2H), 1.84-1.77 (m, 2H), 1.51-1.41 (m, 2H), 1.35-1.26 (m, 24H), 0.88 ppm (t, *J* = 6.8 Hz, *J* = 6.8 Hz, 3H) (Fig. S1); ^{13}C NMR (125 MHz, $CDCl_3$): δ 184.58, 184.13, 162.61, 151.60, 146.66, 129.57, 129.02, 128.41, 128.09, 127.88, 125.78, 124.43, 120.44, 114.40, 91.39, 68.27, 31.93, 29.70, 29.67, 29.60, 29.57, 29.37, 29.15, 26.00, 22.70, 14.13 ppm (Fig. S2); FT-IR (KBr): 2924, 2848, 1587, 1487, 1277, 1254, 1230, 1167, 1119, 1026, 841, 787, 755, 694 cm^{-1}; MALDI-TOF MS, *m/z* (%): calcd for 632.40 $[M+H]^+$, found: 632.51 (100) $[M+H]^+$ (Fig. S3); Elemental analysis for $C_{43}H_{53}NO_3$. Calcd: (%) C, 81.73; H, 8.45; N, 2.22. Found: (%) C, 81.90; H, 8.72; N, 2.29.

(2Z,2'Z)-1,1'-((phenylazanediyl)bis(4,1-phenylene))bis(3-(4-(hexadecyloxy)phenyl)-3-hydroxyprop-2-en-1-one) (2).

By following the synthetic procedure for compound **1**, compound **2** was prepared from compound **5** (1.00 g, 3.04 mmol) and methyl 4-(hexadecyloxy)benzoate (2.74 g, 7.29 mmol) catalyzed by Sodium hydride (60%, 0.49 g, 12.16 mmol). The crude product was purified by column chromatography (silica gel, CH_2Cl_2/petroleum ether, v/v = 3/2), followed by recrystallization from ethanol to give a yellow solid (0.80 g). Yield: 25%. mp: 60.0-62.0 °C. ^{1}H NMR (400 MHz, $CDCl_3$): δ 17.10 (s, 2H), 7.94 (d, *J* = 8.2 Hz, 4H), 7.88 (d, *J* = 8.8 Hz, 4H), 7.37 (t, *J* = 7.6 Hz, *J* = 7.6 Hz, 2H), 7.23-7.15 (m, 7H), 6.96 (d, *J* = 8.8 Hz, 4H), 6.73 (s, 2H), 4.03 (t, *J* = 6.4 Hz, *J* = 6.4 Hz, 4H), 1.84-1.77 (m, 4H), 1.50 -1.43 (m, 4H), 1.37-1.25 (m, 48H), 0.88 ppm (t, *J* = 6.0 Hz, *J* = 7.2 Hz, 6H) (Fig. S4); ^{13}C NMR (125 MHz, $CDCl_3$): δ 185.20, 183.60, 162.79, 150.49, 146.06, 129.89, 129.83, 129.15, 128.51, 127.97, 126.51, 125.43, 122.77, 114.46, 91.71, 68.31, 31.94, 29.71, 29.67, 29.61, 29.57, 29.38, 29.15, 22.71, 14.14 ppm (Fig. S5); FT-IR (KBr): 2922, 2850, 1593, 1490, 1470, 1263, 1231, 1171, 1119, 1026, 843, 783, 755, 698 cm^{-1}; MALDI-TOF MS, *m/z* (%): calcd for 1018.68 $[M+H]^+$, found: 1018.56 (89) $[M+H]^+$ (Fig. S6); Elemental analysis for $C_{68}H_{91}NO_6$. Calcd: (%) C, 80.19; H, 9.01; N, 1.38. Found: (%) C, 80.41; H, 9.23; N, 1.42.

(2Z,2'Z,2''Z)-1,1',1''-(nitrilotris(benzene-4,1-diyl))tris(3-(4-(hexadecyloxy)phenyl)-3-hydroxyprop-2-en-1-one) (3).

By following the synthetic procedure for compound **1**, compound **3** was prepared from compound **6** (1.00 g, 2.69 mmol) and methyl 4-(hexadecyloxy)benzoate (4.56 g, 12.10 mmol) catalyzed by Sodium hydride (60%, 0.65 g, 16.14 mmol). The crude product was purified by column chromatography (silica gel, CH_2Cl_2/petroleum ether, v/v = 3/1), followed by recrystallization from the mixed solvents of CH_2Cl_2 and petroleum ether to afford compound **3** (0.45 g) as a yellow solid. Yield: 12%. mp: 98.0-100.0 °C. ^{1}H NMR (500 MHz, $CDCl_3$, 50 °C): δ 16.95 (s, 3H), 7.93 (t, *J* = 9.0 Hz, *J* = 9.5 Hz, 12H), 7.20 (d, *J* = 8.5 Hz, 6H), 6.95 (d, *J* = 9.0 Hz, 6H), 6.73 (s, 3H), 4.03 (t, *J* = 6.5 Hz, *J* = 6.5 Hz, 6H), 1.83-1.78 (m, 6H), 1.49-1.43 (m, 6H), 1.37-1.23 (m, 72H), 0.87 ppm (t, *J* = 7.0 Hz, *J* = 7.0 Hz, 9H) (Fig. S7); ^{13}C NMR (100 MHz, $CDCl_3$, ppm): δ 185.58, 183.22, 162.90, 149.74, 131.12, 129.23, 128.67, 127.86, 124.10, 114.48, 91.92, 68.32, 31.93, 29.70, 29.67, 29.60, 29.57, 29.14, 26.00, 22.70, 14.13 ppm (Fig. S8); FT-IR (KBr): 2924, 2852, 1593, 1498, 1470, 1319, 1282, 1263, 1228, 1175, 1121, 846, 781 cm^{-1}; MALDI-TOF MS, *m/z* (%): calcd for 1404.97 $[M+H]^+$, found: 1404.68 (100) $[M+H]^+$ (Fig. S9); Elemental analysis for $C_{93}H_{129}NO_9$. Calcd: (%) C, 79.50; H, 9.25; N, 1.00. Found: (%) C, 79.73; H, 9.53; N, 1.05.

6-(4-(diphenylamino)phenyl)-2,2-difluoro-4-(4-(hexadecyloxy)phenyl)-2H-1,3,2-dioxaborinin-1-ium-2-uide (1B).

Compound **1** (1.00 g, 1.58 mmol) was dissolved in dry CH_2Cl_2 (50 mL) to give a green solution. Then boron trifluoride-diethyl etherate (0.40 mL, 3.16 mmol) were added under an atmosphere of nitrogen via syringe. The reaction mixture was heated to reflux for 4 h. After removal of the solvent, the crude product was purified by column chromatography (silica gel, CH_2Cl_2/petroleum ether, v/v = 1/1), followed by recrystallization from the mixed solvents of THF and ethanol to afford compound **1B** (0.62 g) as an orange solid. Yield: 58%. mp: 74.0-76.0 °C. ^{1}H NMR (400 MHz, $CDCl_3$): δ 8.07 (d, *J* = 8.8 Hz, 2H), 7.95 (d, *J* = 9.2 Hz, 2H), 7.37 (t, *J* = 8.0 Hz, *J* = 7.6 Hz, 4H), 7.24-7.19 (m, 6H), 6.99-6.97 (m, 4H), 6.93 (s, 1H), 4.05 (t, *J* = 6.8 Hz, *J* = 6.4 Hz, 2H), 1.85-1.78 (m, 2H), 1.50-1.43 (m, 2H), 1.36-1.26 (m, 24H), 0.88 ppm (t, *J* = 6.8 Hz, *J* = 6.8 Hz, 3H) (Fig. S10); ^{13}C NMR (125 MHz, $CDCl_3$): δ 179.89, 179.50, 164.62, 153.92, 145.60, 130.93, 130.68, 129.86, 126.56, 125.71, 124.54, 123.00, 118.71, 114.87, 91.17, 68.58, 31.93, 29.70, 29.60, 29.55, 29.36, 29.05, 25.96, 22.70, 14.13 ppm (Fig. S11); FT-IR (KBr): 2920, 2850, 1554, 1500, 1340, 1248, 1178, 1036, 846, 798, 758, 696 cm^{-1}; MALDI-TOF MS, *m/z* (%): calcd for 680.40 $[M+H]^+$, found: 680.50 (100) $[M+H]^+$ (Fig. S12); Elemental analysis for $C_{43}H_{52}BF_2NO_3$. Calcd: (%) C, 75.99; H, 7.71; N, 2.06. Found: (%) C, 76.21; H, 7.86; N, 2.09.

6,6'-((phenylazanediyl)bis(4,1-phenylene))bis(2,2-difluoro-4-

(4-(hexadecyloxy)phenyl)-2H-1,3,2-dioxaborinin-1-ium-2-uide) (2B).

By following the synthetic procedure for compound **1B**, compound **2B** was prepared from compound **2** (1.00 g, 0.71 mmol) and boron trifluoride-diethyl etherate (0.54 mL, 4.26 mmol). The crude product was purified by column chromatography (silica gel, CH_2Cl_2/petroleum ether, v/v = 7/4), followed by recrystallization from the mixed solvents of THF and ethanol to afford **2B** (0.31 g) as an orange solid. Yield: 95%. mp: 168.0-170.0 °C. ^{1}H NMR (400 MHz, $CDCl_3$): δ 8.11 (d, J = 8.8 Hz, 4H), 8.04 (d, J = 8.8 Hz, 4H), 7.44 (t, J = 8.0 Hz, J = 7.2 Hz, 2H), 7.32 (t, J = 7.2 Hz, J = 7.2 Hz, 1H), 7.2-7.18 (m, 6H), 7.00-6.99 (m, 6H), 4.07 (t, J = 6.4 Hz, J = 6.4 Hz, 4H), 1.86-1.79 (m, 4H), 1.49-1.44 (m, 4H), 1.36-1.26 (m, 48H), 0.88 ppm (t, J = 5.6 Hz, J = 7.2 Hz, 6H) (Fig. S13); ^{13}C NMR (125 MHz, $CDCl_3$): δ 180.98, 179.58, 165.19, 152.00, 144.89, 131.39, 130.50, 130.34, 127.24, 126.93, 126.47, 124.12, 122.62, 115.04, 91.82, 68.70, 31.94, 29.71, 29.71, 29.60, 29.56, 29.37, 29.04, 25.96, 22.70, 14.13 ppm (Fig. S14); FT-IR (KBr): 2924, 2852, 1547, 1496, 1375, 1244, 1178, 1035 cm^{-1}. MALDI-TOF MS, *m/z* (%): calcd for 1114.68 $[M+H]^+$, found: 1114.88 (65) $[M+H]^+$ (Fig. S15); Elemental analysis for $C_{68}H_{89}B_2F_4NO_6$. Calcd: (%) C, 73.31; H, 8.05; N, 1.26. Found: (%) C, 73.56; H, 8.24; N, 1.23.

6,6',6''-(nitrilotris(benzene-4,1-diyl))tris(2,2-difluoro-4-(4-(hexadecyloxy)phenyl)-2H-1,3,2-dioxaborinin-1-ium-2-uide) (3B).

By following the synthetic procedure for **1B**, **3B** was prepared from **3** (1.00 g, 0.71 mmol) and boron trifluoride-diethyl etherate (0.54 mL, 4.26 mmol). The crude product was purified by column chromatography (silica gel, CH_2Cl_2/petroleum ether, v/v = 3/1), followed by recrystallization from the mixed solvents of THF and ethanol to afford **3B** (0.99 g) as an orange solid. Yield: 90%. mp: 116.0-118.0 °C. ^{1}H NMR (400 MHz, $CDCl_3$): δ 8.05 (t, J = 9.6 Hz, J = 9.6 Hz, 12H), 7.20 (d, J = 8.4 Hz, 6H), 7.04 (s, 3H), 6.94 (d, J = 8.8 Hz, 6H), 4.03 (t, J = 6.4 Hz, J = 6.4 Hz, 6H), 1.85-1.78 (m, 6H), 1.47-1.43 (m, 6H), 1.36-1.26 (m, 72H), 0.87 (t, J = 7.6 Hz, J = 7.6 Hz, 9H) (Fig. S16); ^{13}C NMR (100 MHz, $CDCl_3$): δ 181.7, 179.2, 165.5, 150.9, 131.6, 130.6, 128.3, 124.5, 123.8, 115.1, 92.2, 68.8, 31.9, 29.7, 29.7, 29.6, 29.6, 29.4, 29.0, 26.0, 22.7, 14.1 ppm (Fig. S17); FT-IR (KBr): 2924, 2852, 1547, 1491, 1371, 1273, 1242, 1176, 1128, 1038, 847, 796 cm^{-1}; MALDI-TOF MS, *m/z* (%): calcd for 1528.96 $[M-F]^+$, 1548.96 $[M+H]^+$, found: 1529.03 (100) $[M-F]^+$, 1548.90 (20) $[M]^+$ (Fig. S18); Elemental analysis for $C_{93}H_{126}B_3F_6NO_9$. Calcd: (%) C, 72.14; H, 8.20; N, 0.90. Found: (%) C, 72.40; H, 8.48; N, 0.83.

Results and discussion

Synthesis and characterizations

The synthetic routes for triphenylamine functionalized β-diketones **1-3** and the corresponding difluoroboron β-diketonate complexes **1B-3B** were shown in Scheme 2. Firstly, the triphenylamine bearing different numbers of acetyl groups **4-6** were synthesized via Friedel-Crafts acylation reactions according to the literature.[17] Then, β-diketonates **1-3** were synthesized via Claisen condensation reactions between methyl 4-(hexadecyloxy)benzoate and the corresponding ketones **4-6** in the presence of sodium hydride in anhydrous THF, followed by acidification with dilute HCl, respectively, in yields of 49%, 25% and 12%. It should be noticed that THF used in reaction must be anhydrous, otherwise, the yield would be reduced remarkably because 4-(hexadecyloxy)benzoate would be hydrolyzed to 4-(hexadecyloxy)benzoic acid. From ^{1}H NMR spectrum of each β-diketone (Fig. S1, S4 and S7), we could observe a single peak emerged around 17 ppm assigned to the chemical shift of the hydrogen in hydroxyl group, indicating the existence of enol form.[19,11c] Additionally, only a small amount of molecules existed in ketone form, which supported by the appearance of weak signal at 4.5 ppm due to the proton in methylene in ^{1}H NMR spectra. Moreover, we could find some weak peaks in the range of 6.7-8.1 ppm, which were ascribed to the protons in aromatic rings in ketone forms of **1-3**. Finally, the complexes **1B-3B** could be easily prepared via the complex of β-diketone ligands **1-3** with boron trifluoride-diethyl etherate. The target molecules were characterized by ^{1}H NMR and ^{13}C NMR spectroscopies, MALDI-TOF mass spectrometry, FT-IR spectroscopy and C, H, N elemental analyses.

Photophysical properties and quantum chemical calculations

The UV-vis absorption spectra of **1-3** and **1B-3B** in toluene were shown in Fig. 1a, and the corresponding photophysical data were summarized in Table S1. It was clear that the maximal absorption bands of β-diketones **1-3** were located at 408 nm, 427 nm and 422 nm, respectively, whose molar absorption coefficients (ε_{max}) increased with the increase of the number ofβ-diketone unit. For example, the ε_{max} value of the absorption at 408 nm was 4.22 × 10^{-4} M^{-1}cm^{-1} for compound **1**, and reached 10.28 × 10^{-4} M^{-1}cm^{-1}

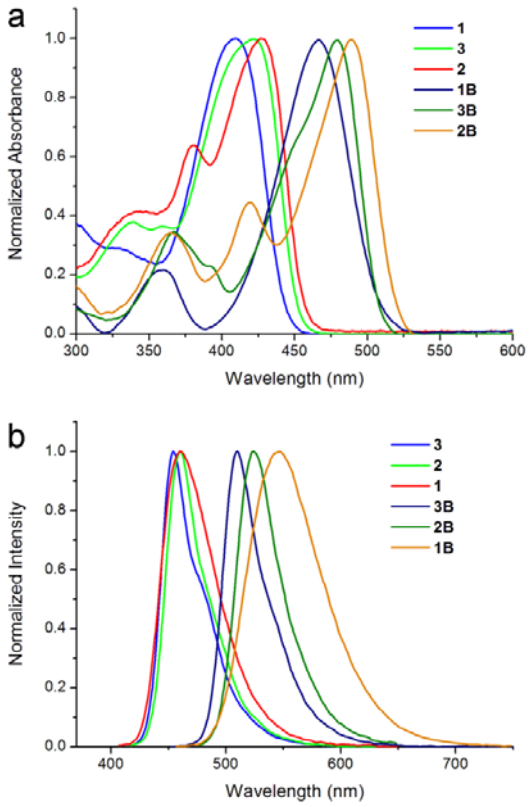

Fig. 1 Normalized UV-vis absorption (a) and fluorescence emission (b, λ_{ex} = 400 nm for **1-3**, 450 nm for **1B-3B**) spectra of **1-3** and **1B-3B** in toluene (2.0 × 10^{-6} M).

of the absorption at 422 nm for compound **3**, meaning strong light harvesting abilities. Compared with ligands**1-3**, the difluoroboron β-diketonate complexes **1B-3B** showed similar but red-shifted absorption bands. The maximual absorption bands for **1B-3B** emerged at 467 nm, 490 nm and 479 nm, respectively. Meanwhile, the molar absorption coefficients of the maximum absorption peaks for **1B-3B** were higher than the corresponding ligands **1-3**, and they also increased with the increasing number of difluoroboron β-diketonate units. For example, the molar absorption coefficient of **3B** increased to 15.62×10^4 $M^{-1}cm^{-1}$ at 479 nm from 6.21×10^4 $M^{-1}cm^{-1}$ at 467 nm for **1B**.

Owing to the electron donating ability of triphenylamine and the electron accepting ability of β-diketone or difluoroboron β-diketone moieties, the maximal absorption band can be ascribed to the ICT transition, which could be supported by the solvent-dependent fluorescence emission spectral changes (Fig. S19-S20, Table S2-S3).[7d,16b,20] We found that the fluorescence emission bands of six compounds red-shifted significantly with increasing the solvent polarity, accompanying with the increase of stokes shifts and the broaden of the emission. To get an insight into the absorption spectra of the six compounds, density functional theory (DFT) was used to calculate the electronic structures and time-dependent DFT (TD-DFT) was adopted to investigate the electronic transitions on the optimized ground-state geometries. All calculations were performed at B3LYP/6-31G level with the Gaussian 09W program package.[21] From Table 1 we could find a well quantitative agreement of λ_{abs} values between the experimental and the calculated data. In the cases of compounds **1-2** and **1B-2B**, the maximal absorption band originated from the electronic transition of HOMO→LUMO. For compounds **3** and **3B**, the maximal absorption came from two kinds of transitions of HOMO→LUMO and HOMO→LUMO+1 since the energy levels of LUMO and LUMO+1 were so close ($\Delta E < 0.01$ eV) that the two transitions overlapped completely.[22] Similar phenomenon was also observed for the absorption at 339 nm of compound **3** because the energy levels of HOMO-1 and HOMO-2 were almost same (Fig. S21). Moreover, the calculated oscillator strength of **1-3** increased with increasing number of β-diketone units, and was lower than the corresponding difluoroboron complexes (Table 1), consisting with the data of the absorption coefficients. Fig. 2 showed the plots of molecular orbitals involved in the maximal absorption of **1-3** and **1B-3B**. It was clear that the π-electrons in HOMO for compounds **1-3** and **1B-3B** were mainly delocalized over the triphenylamine units, while LUMO and LUMO+1 were mainly delocalized over β-diketone (for **1-3**) or difluoroboron β-diketone (for **1B-3B**) moieties. Thus, the maximal absorption band could be assigned to ICT transition.[23] The transition component of other absorption bands were also listed in Table 1 and the corresponding plots of frontier orbitals were shown in Fig. S21. For example, the absorption band at 330 nm of **1** and 359 nm of **1B** both originated from the electronic transition of HOMO-1, where π-electrons were mainly delocalized over the hexadecyloxyphenyl fragments, to LUMO. The electron-donating ability of hexadecyloxy benzene was weaker than triphenylamine, so the corresponding absorption bands resulted from HOMO-1→LUMO were located at higher energy region compared with the maximum absorption bands. The fact that the absorption intensities of the transition from HOMO-1 to LUMO were lower than those of maximum absorption bands were related to the values of calculated oscillator strength. Moreover, we found from Fig. 2 that the LUMO and HOMO energy levels of the six compounds decreased in a order of **1**, **2**, **3**, **1B**, **2B** and **3B** on account of the gradually increased electron-withdrawing abilities of the acceptors. The calculated energy gaps of six compounds were ranked in an order of **1** > **3** > **2** > **1B** > **3B** > **2B**, which were in accordance with their absorption bands.

Table 1. Main orbital transitions calculated with TD-DFT.

compound	λ_{abs} [a]/ nm	λ_{cal} [b]/ nm	f [c]	Composition (%) [d]
1	408	422.10	0.8189	H → L (98)
	330	336.07	0.5514	H-1 → L (90)
2	427	445.38	1.1376	H → L (97)
	380	400.09	0.2607	H → L+1 (99)
	340	350.57	0.2322	H-1 → L (99)
3	422	442.72	1.0498	H → L (97)
		442.18	1.0657	H → L+1 (97)
	339	354.93	0.3814	H-2 → L (24)
				H-2 → L+1 (18)
				H-1 → L (29)
				H-1 → L+1 (25)
		354.84	0.3809	H-2 → L (26)
				H-2 → L+1 (19)
				H-1 → L (30)
				H-1 → L+1 (22)
1B	467	463.02	1.0123	H → L (99)
	359	351.87	0.5442	H-1 → L (95)
2B	490	497.47	1.3846	H → L (98)
	419	431.52	0.3287	H → L+1 (98)
	365	376.30	0.3653	H-1 → L (99)
3B	479	488.22	1.0937	H → L (98)
		486.52	1.1333	H → L+1 (98)
	367	378.54	0.3759	H-2 → L+1 (21)
				H-1 → L (77)
		377.95	0.3964	H-2 → L (50)
				H-1 → L+1 (48)

[a] Measured absorption band in toluene. [b] Calculated electronic transition band in vacuo. [c] Calculated oscillator strength in vacuo. [d] H represents HOMO, L represents LUMO.

The fluorescence emission spectra of **1-3** and **1B-3B** in toluene were shown in Fig. 1b. β-Diketone **1** exhibited intense blue fluorescence located at 462 nm, and the fluorescence quantum yield (Φ_f) was 0.53 using diphenylanthracene as reference. Similarly, compounds **2** and **3** gave blue light emission centered at 460 nm and 454 nm, respectively, and the Φ_f were as high as 0.57 and 0.54, rspectively. In the cases of difluoroboron β-diketone complexes **1B-3B**, the emission red-shifted to 547 nm, 525 nm and 510 nm, respectively, and Φ_f were in the range of 0.60-0.82 using fluorescein as reference. Therefore, the obtained β-diketones and difluoroboron complexes were high emissive in toluene. Moreover, remarkabe red-shift of the emission bands for

Cite this: DOI: 10.1039/c0xx00000x

www.rsc.org/xxxxxx

ARTICLE TYPE

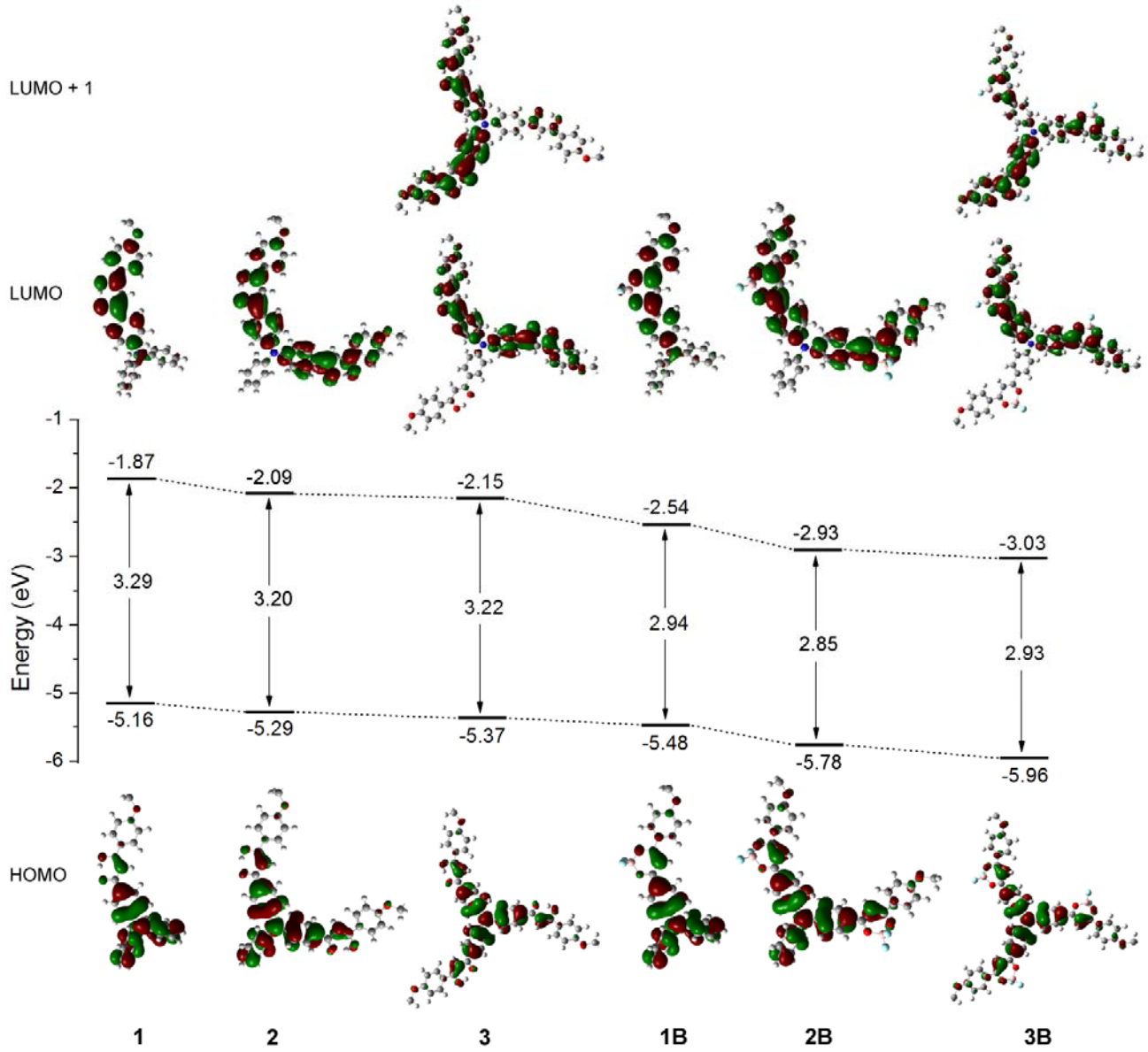

Fig. 2 Energy levels and molecular orbital surfaces in the optimized ground-state structures of **1-3** and **1B-3B**, in which hexadecyl groups were omitted.

the six compounds were observed in solid states compared with those in toluene due to intermolecular π-π interactions (Table S1). For example, compound **3** emitted green light (517 nm) and **3B** emitted orange light (604 nm) in soid states. The Φ_f of six compounds in solid state were measured using an integrating sphere. Notably, the Φ_f of **3B** in solid state reached 0.66, which was one of strong orange light solid emitting dyes. [24] Compound **1** also gave high Φ_f of 0.43 in solid state. Although the Φ_f for other four compounds were in the range of 0.10-0.25, they could be considered as solid emitting dyes.[24a,25] As a result, strong emission for **1-3** and **1B-3B** in solid state made them possible be applied in emitting materials.

Gelation abilities of 1-3 and 1B-3B

The gelation behaviors of β-diketones **1-3** and difluoroboron β-diketone complexes **1B-3B** were investigated in various solvents by using the ”stable to inversion of a test tube” method,[1b,3d] and the results were summarized in Table 2. It was found that only compound **2** was unable to gelate any of the tested solvents, whereas other compounds exhibited gelation abilities. Among them, compounds **1**, **3**, **1B** and **2B** could form gels in more polar solvents. For example, **1** and **1B** could gelate DMSO and DMSO/H_2O (v/v = 15/1) via heating-cooling process, additionally, **1B** could form gels in CH_3COOH and

CH_3COOH/H_2O (v/v = 30/1, 10/1) under ultrasound stimulation. Compound **2B** could form gel only in DMSO, and **3** exhibited gelation abilities in DMAc, acetone and DMF. However, **3B** could form gels in nonpolar aliphatic hydrocarbon solvents, such as petroleum, *n*-hexane, and *n*-heptane. Since the π-conjugation of **2** may be larger than **1** due to the introduction of two β-diketone units, **2** might prefer to precipitate from organic solvents because of strong π-π interaction and no gel was formed.[16a,26] Although the three β-diketone units were introduced, **3** showed gelation ability. The reasons might be that, on the one hand, the dihedral angle in **3** between two β-diketone groups was larger than that in **2** (Fig. S22-S23), leading to weaker conjuation degree of **3** than **2**. On the other hand, the three long alkyl chains in *C3*-symmetric molecule would favor the self-assemble into organogel.[27] Hence, it was understandble that **1** and **3** could form gels but **2** could not. However, **2B** with similar molecular structure to **2** could form gel because the polarity of **2B** was higher than **2**. Thus, the dipole-dipole interaction should be one of driving forces for the gelation of difluoroboron β-diketone complexes. Compared with compounds **1B** and **3B**, **2B** showed weak gelation ability since it could only form gel in DMSO and gave relatively high critical gelation concentration (CGC). It could be explained by similar reason for the different gelation abilities of **1-3** (Fig. S24-S25).

The obtained gels were stable for several weeks at room temperature and could be destroyed when heated. However, the organogels could be recovered after the hot solutions were cooled naturally or stimulated by ultrasound. The photographs of selected organogels were shown in Fig. S26.

Self-assembling properties in gel states

To get an insight into the morphologies of the self-assemblies of **1**, **3**, **1B**-**3B** in gel states, the scanning electron microscopy (SEM) and fluorescence microscopy images were shown in Fig. 3. It was found that the morphologies of xerogels were dependent on the molecular configuration. For example, numerous straight nanofibers in length of micrometer and in width of ca. 200 nm were generated in the xerogel **1** obtained from DMSO (Fig. 3a-b). Similarly, Fig. 3e-f illustrated that three-dimensional networks consisting numerous straight nanofibers in width of 100-500 nm and in length of tens of micrometer were formed in xerogel **1B** obtained from CH_3COOH/H_2O = 10/1. Therefore, the asymmetric β-diketone **1** and its difluoroboron complex **1B** tended to assemble into straight nanofibers. From the SEM image of xerogel **3** obtained from DMF we found lots of entangled fibers with diameter of ca. 100 nm, and some thinner fibers twisted together into bundles with a width of 1-1.5 μm (Fig. 3c). It was interesting that some helical fibers were formed from *C3*-symmetric compound **3** (see Fig. S27 and S28). It can be seen that right- and left-handed helices were present, thus resulting in overall racemic mixtures. It could be confirmed by the absence of any CD signal of gel **3** (Fig. S29). The reason why the helical fibers formed would be discussed below. With similar molecular architecture to **3**, compound **3B** self-assembled into ill-defined agglomerates, but 3D networks with a lot of mesh could be observed. In xerogel **2B**, dendritic structures composed of numerous nanofibers in width of 200-800 nm and in length of several micrometer appeared (Fig. 3g-i).

In order to obtain the information on the organization of fluorophores during the gel formation, the temperature-dependent electronic spectra were shown in Fig. 4. It was found that during the gelation process the maximal absorption at 418 nm of compound **1** in hot DMSO decreased gradually and blue-shifted to 410 nm in gel state, indicating the formation of *H*-aggregates in gel state.[28] Meanwhile, the fluorescent emission band of **1** exhibited a large blue-shift from 551 nm in hot solution to 504 nm in gel phase (Fig. 4b). Accordingly, it was clear as shown in the inset in Fig. 4b that the emitting color changed from yellow to green (Fig. 3a) during the sol-gel transition. Interestingly, achieved during the gelation of **1**,[29] whose fluorescence emission intensity increased obviously upon cooling the hot DMSO solution to room temperature. Generally, the fluorescence emission band of D-π-A compounds would red-shift and its

Table 2. Gelation abilities of ligands **1-3** and complexes **1B-3B** in organic solvents.

Solvent	**1**	**2**	**3**	**1B**	**2B**	**3B**
Petroleum	S	P	P	S	I	G (14.3)
n-Hexane	S	P	P	S	I	G (10.5)
n-Heptane	S	P	P	S	I	G (6.9)
Cyclohexane	S	S	P	S	I	S
Toluene	S	S	S	S	S	S
DCM	S	S	S	S	S	S
THF	S	S	S	S	S	S
Ethanol	P	I	P	P	I	I
DMAc	S	P	G (20.0)	S	P	S
Acetone	S	P	G (12.5)	S	P	S
DMF	P	P	G (6.7)	S	P	S
DMSO	G (2.8)	I	I	G (16.7)	G (25.0)	P
$DMSO/H_2O$ (v/v = 15/1)	G (2.5)	I	I	G (9.1)	I	P
CH_3COOH	P	I	I	G (6.7)[a]	I	I
CH_3COOH/H_2O (v/v = 30/1)	P	I	I	G (3.2)[a]	I	I
CH_3COOH/H_2O (v/v = 10/1)	P	I	I	G (1.4)[a]	I	I

G: gel, **S**: soluble, **I**: insoluble, **P**: precipitation. The critical gelation concentration (CGC) is shown in parentheses (mg mL^{-1}).
[a] Gelation was induced by ultrasound stimulation.

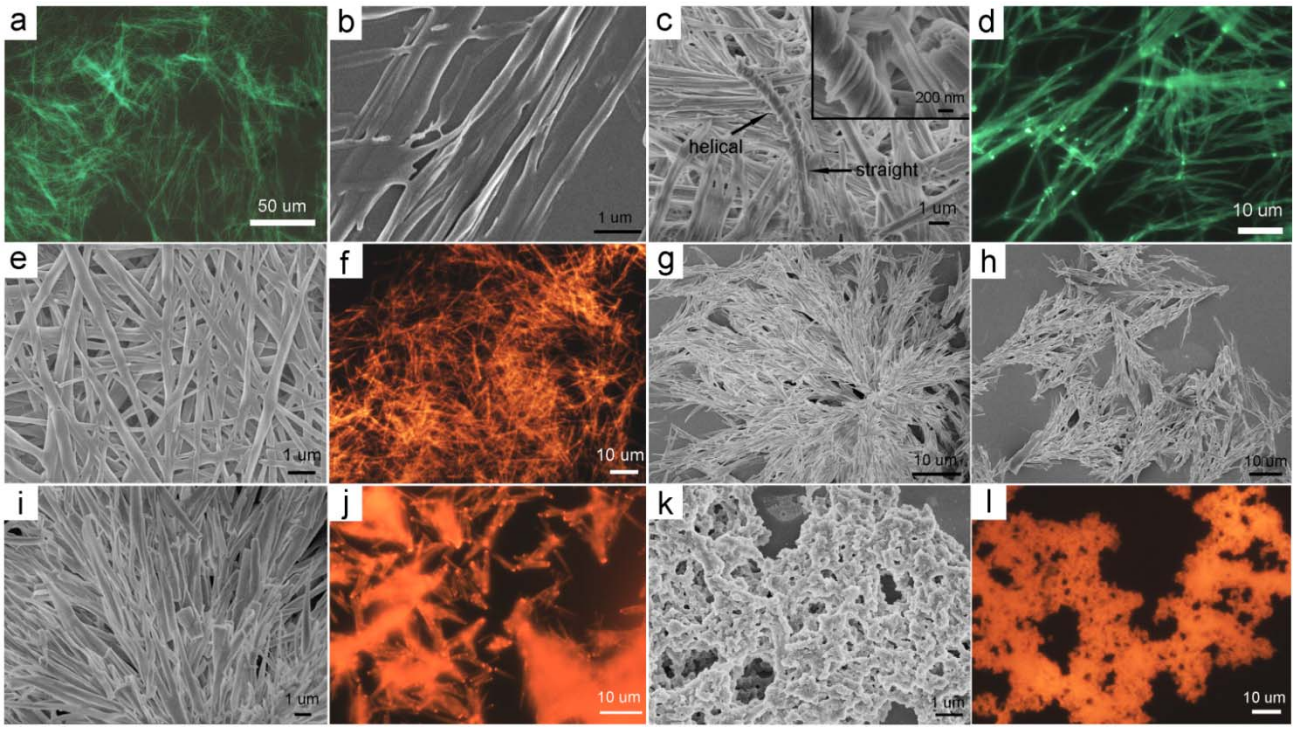

Fig. 3 (a) Fluorescence microscopy and (b) SEM images of the gel of **1** in DMSO; (c) SEM and (d) Fluorescence microscopy images of the gel of **3** in DMF, the inset (c) shows the amplified helical fibers; (e) SEM and (f) Fluorescence microscopy images of the gel of **1B** in CH_3COOH/H_2O = 10/1; (g-i) SEM and (j) Fluorescence microscopy images of the gel of **2B** in DMSO; (k) SEM and (l) Fluorescence microscopy images of the gel of **3B** in heptane.

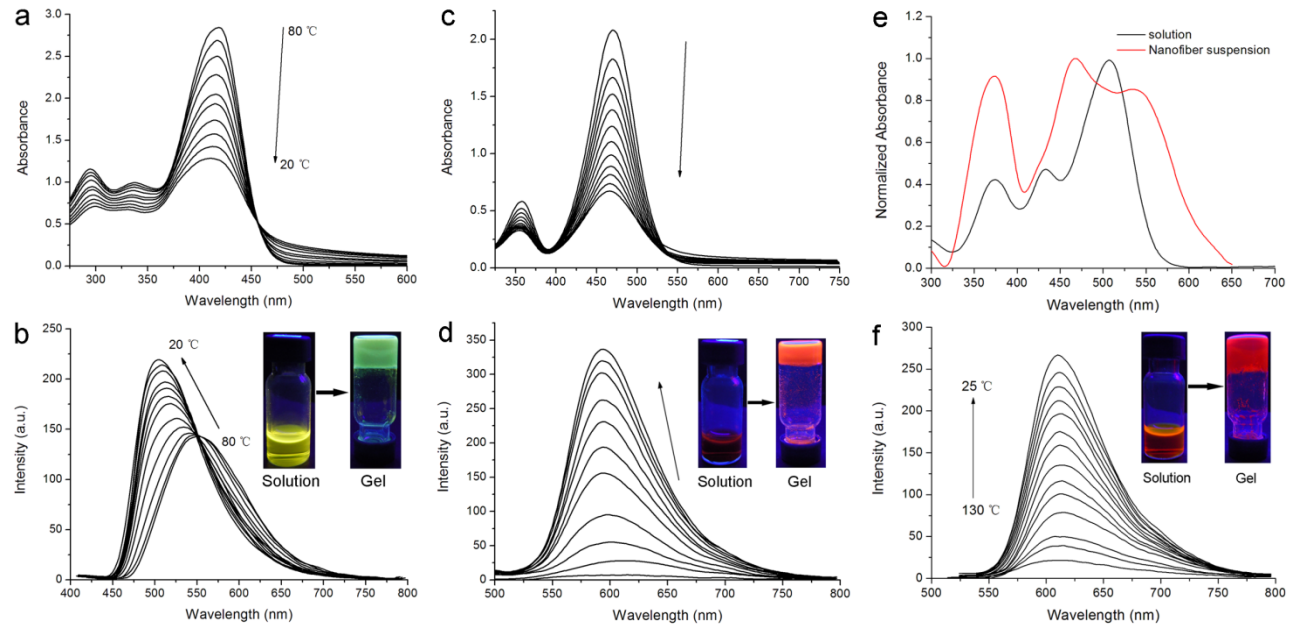

Fig. 4 Temperature-dependent UV-vis absorption (a) and fluorescence emission (b) spectra (λ_{ex} = 400 nm) of **1** in DMSO; Time-dependent UV-vis absorption (c) and fluorescence emission (d) spectra (λ_{ex} = 460 nm) of **1B** upon aging the solution in CH_3COOH/H_2O (v/v = 10/1, 2.3 × 10^{-3} mol/L) after ultrasound treatment; (e) Normalized UV-vis absorption spectra of **2B** in DMSO (2×10^{-6} M) and in the gel dipersed in hexane; (f) Temperature-dependent fluorescence emission spectra of **2B** in DMSO（λ_{ex} = 500 nm）. Inset: photos of the solutions and gels irradiated by 365 nm light. The arrows indicate the spectral changes from the solution to gel.

emission intensity decrease in strong polar solvents compared with in nonpolar solvents because of the dipole-dipole interactions between the excited molecules and solvent molecules. In this case, we suggested that the blue-shift and the enhanced intensity of the fluorescence emission for **1** during the gel formation were due to the removal of DMSO molecules from the aggregates. In other words, the fluorescence quenching caused by solvent molecules was suppressed in gel state.[9a,30] The UV-vis absorption and fluorescent emission spectra of **1B** in CH_3COOH/H_2O (v/v = 10/1) upon cooling the hot solutions, which was first stimulated by ultrasound, to room temperature were shown in Fig. 4c-d. We could find that the maximal

absorption band at 470 nm blue-shifted to 466 nm, accompanying with the decrease of the absorption intensity during the gelation process. Therefore, π-π interactions played a key role in the gel formation of **1B**. As shown in Fig. 4d, the emission at ca. 612 nm for **1B** in hot solution was very weak, and it blue-shifted gradually upon gelation, accompanying with the obvious increase of the emission intensity. In the gel state, the emission of **1B** shifted to 594 nm, emitting strong orange light (inset in Fig. 4d and Fig. 3f), and ca. 33 times of the emission enhancement was achieved compared with that in hot solution. Since the absorption of **2B** in DMSO at the concentration over CGC (25.0 mg/mL) was out of the range of the equipment, gel **2B** was dispersed in a poor solvent (hexane), in which the nanofibers formed in gel could be maintained to a great extent, for UV-vis absorption measurement [3e]. It was clear from Fig. 4e that the absorption bands at 433 nm and 468 nm for **2B** in dilute DMSO red-shifted to 507 nm to 538 nm, respectively, in the gel nanofibers. It suggested that the *J*-aggregates were formed via π-π interaction in nanofibers of **2B**. Meanwhile, the emission intensity of **2B** increased significantly without shift upon cooling the hot solution in DMSO to room temperature (Fig. 4f), and the gel could emit intense red light centered at 611 nm (inset in Fig. 4f and Fig. 3j).

Although the emission intensities of **3** and **3B** in gels were lower than those in solutions, the obtained gels still emitted strong green and orange light, respectively (Fig. 5b and 5d, Fig. 3d and 3l). Firstly, the broaden and slight red-shift of the absorption peaks of **3** and **3B** in gel states compared with those in solutions indicated that π-π aggregates were formed in gel state (Fig. 5a and 5c). Secondly, during the gel formation, the obvious decrease of the fluorescent emission intensity of **3**, and slight red-shift (from 582 nm to 590 nm) as well as slight decrease of the emission for **3B** also illustrated that π-πinteractions were main driving forces for the gels formation of **3** and **3B**.

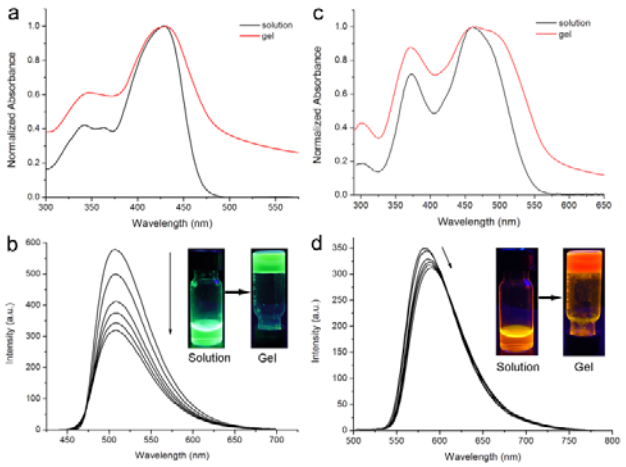

Fig. 5 Normalized UV-vis absorption spectra of **3** in solution (2×10^{-6} M) as well as in gel state in DMF (a) and **3B** in solution (2×10^{-6} M) as well as in gel state in heptane (c), temperature-dependent fluorescence emission spectra of **3** in DMF (b, λ_{ex} = 430 nm) and **3B** in heptane (d, λ_{ex} = 470 nm). Inset: photos of the gels and corresponding solutions irradiated by 365 nm light. The arrows indicate the spectral changes from the solution to gel.

As representative examples, temperature-dependent ^{1}H NMR spectra of **1** and **1B** in DMSO-d_6 were recorded to further probe the driving forces for the gelation. As shown in Fig. 6a, the ^{1}H NMR spectrum of **1** gave weak and ill-resolved resonance signals due to the restricted freedom of thermal motion of the organic molecules in the gel state at 20 °C. As the temperature increased, all the signals in the ^{1}H NMR spectra became well-resolved, and chemical shift variations of some signals were observed. For example, the signals of H_a at 8.08 ppm and H_b at 8.01 ppm shifted upfield to 8.02 and 7.95 ppm, respectively, at 80 °C. Meanwhile, the signal of H_c in β-diketone shifted upfield from 7.12 to 6.99 ppm. The resonance signals of H_d, H_e and H_f in **1B** were also shifted upfield from 8.27, 8.19, 7.60 ppm at 20 °C to 8.21, 8.14, 7.46 ppm at 80 °C, respectively. These temperature-dependent changes of chemical shifts of the protons in aromatic rings illustrated that π-π interactions were main driving forces for the self-assembling of the gelator molecules.[31]

In order to reveal the molecular packing modes in gel phases, the XRD patterns of the xerogels were shown in Fig. S30-S31. As to xerogel **1**, we could find four diffraction peaks corresponding to *d*-spacing of 4.02 nm, 1.94 nm, 1.29 nm and 0.99 nm, which were close to a ratio of 1:1/2:1/3:1/4. It indicated a layered structure with long period of 4.02 nm was generated in the gel **1**.[7a,b,c,32] Moreover, the molecular length of **1** in optimized

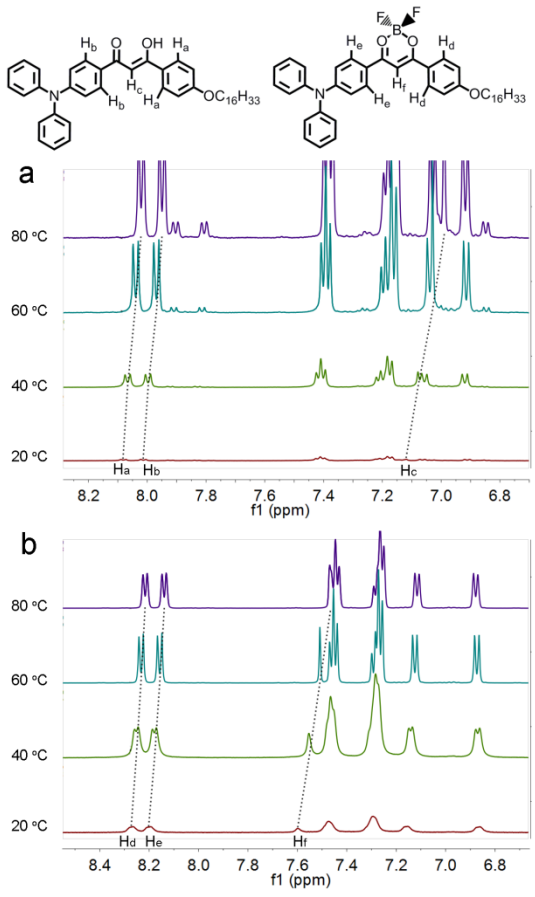

Fig. 6 Temperature-dependent ^{1}H NMR spectra of **1** in DMSO-d_6 at 3.6 mg mL^{-1} (a) and **1B** in DMSO-d_6 at 18.2 mg mL^{-1} (b).

Cite this: DOI: 10.1039/c0xx00000x

www.rsc.org/xxxxxx

ARTICLE TYPE

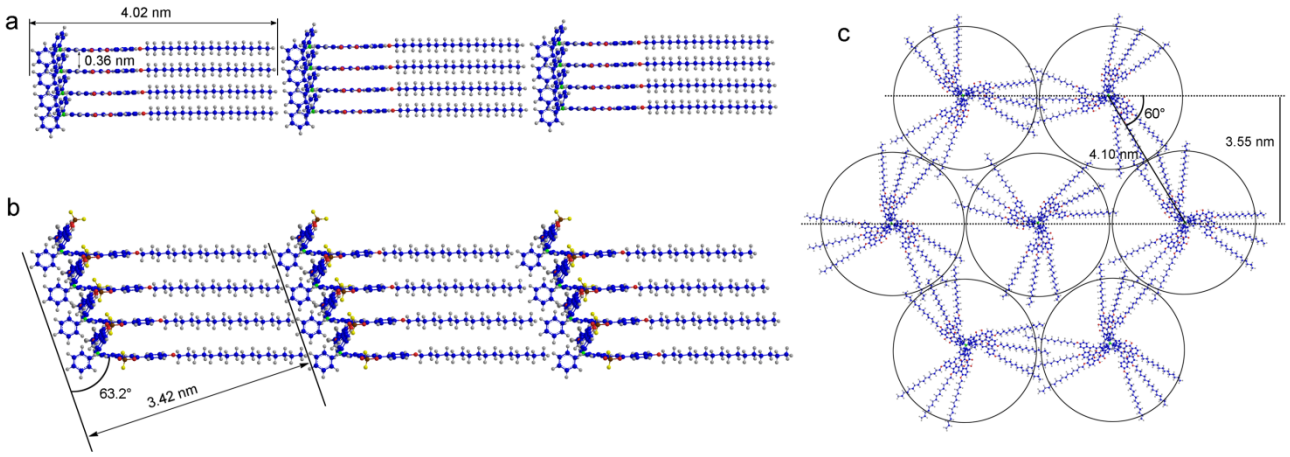

Fig. 7 Proposed molecular packing models of **1** and **1B** (a), **2B** (b) and **3** (c) in gel phases.

geometry based on DFT calculation was 3.85 nm (Fig. S32), so we suggested that **1** arranged into a lamellar structure using the molecular length as the long period in gel state. The proposed molecular packing mode was illustrated in Fig. 7a, in which *H*-aggregates were formed in gel state, in accordance with the results of temperature-dependent UV-vis absorption spectra. XRD pattern of **1B** in xerogel showed two peaks corresponding to *d*-spacing of 4.02 nm and 2.00 nm, which were close to a ratio of 1:1/2. It is understandable that **1B** also arranged into a layered structure using the molecular length as the long period in gel state, which was similar to that of **1** due to their similar molecular structures. In addition, in the wide-angle region xerogels **1** and **1B** gave several peaks, in which one peak at 24.4 degree corresponded to a *d*-spacing of 0.36 nm. It was a characteristic of a typical π-π stacking distance.[7e,h] It meant that π-π interaction took place in gel state. In the XRD pattern of xerogel **2B**, only one sharp peak corresponding to a *d*-spacing of 3.42 nm could be detected in small-angle region. By comparing with the molecular length of **2B** (3.83 nm, Fig. S29), it was inferred that the molecules were stacked over each other in a lamellar structure with a tilt angle of 63.2° in the gel state (Fig. 7b), where *J*-aggregates were involved. The XRD pattern of xerogel **3** exhibited four peaks in small-angle region. The corresponding *d*-spacing was 3.55 nm, 2.05 nm, 1.77 nm and 1.35 nm in the ratio of 1:1/√3:1/√4:1√7, suggesting the formation of a hexagonal columnar structure with the column diameters of 4.10 nm.[33] Combined with the XRD data and the optimized molecular conformation, the reason for the generation of helical fibers from **3** could be deduced. It was known that the core of the triphenylamine was non-coplanar and the dihedral angle between the benzene ring was about 68° in the monomeric state derived from the DFT calculations. Although the dihedral angle between the benzene ring would be decreased in the assembling process, the rotation of phenyl rings would preclude the co-facial alignment of the cores (Fig. S33). Therefore, the cores would be arranged into a propeller-like conformation, leading to helices during gelation. The perfect arrangement of the propeller-like π-conjugated cores would lead to the straight fibers, while the helical fibers would be gained if the conformation of the π-cores was distorted by external stimulation.[27a] On the other hand, the column diameter (4.10 nm) based on XRD results was less than the diameter of molecule **3** (6.61 nm) calculated from the optimized structure (Fig. S29), so it was reasonable that the long carbon chains in the gelator molecule might insert each other partially in adjacent molecules, the stacking mode of xerogel **3** was illustrated in Fig. 7c and S18. No diffraction peak was detected for xerogel **3B**, which suggested amorphous arrangement in gel state. This result was consistent with the SEM image of xerogel **3B**.

Conclusions

A series of new triphenylamine functionalized β-diketones **1-3** and their difluoroboron complexes **1B-3B** were synthesized. It was found that the obtained compounds were highly emissive in toluene. It should be noted that the Φ_f of **3B** in solid state reached 0.66, which was one of strong solid orange light emitting dyes. In addition, the self-assembling properties of the synthesized compounds were dependent on the molecular structures. Although bis-β-diketone substituted triphenylamine **2** could not form organogel, its difluoroboron complex **2B** could gel DMSO due to the strong dipole-dipole interactions. Compounds **1**, **1B** and **3** could form gels in polar solvents, while **3B** formed gels in nonpolar solvents. It is interesting that AIEE was achieved during the gelation of **1**, **1B** and **2B** with asymmetric structures, and the emission of symmetric compounds **3** and **3B** decreased to a certain degree upon gelation. The obtained gels based on compounds **1** and **3** emitted strong green light and gels based on **1B-3B** emitted strong orange or red light. The temperature-dependent UV-vis absorption, fluorescence and ^{1}H NMR spectral data suggested that π-π interactions played a key role in the gel

formation. Meanwhile, the dipole-dipole interactions were one of the driving forces for the gelation of difluoroboron β-diketone complexes. Combined with XRD pattern of the xerogels and the calculated molecular length, the molecular packing modes were proposed in the gels of **1**, **1B**, **2B** and **3**. These highly fluorescent nanostructures might have potential applications in emitting devices and fluorescent sensors.

Acknowledgement

This work was supported by the National Natural Science Foundation of China (21374041), Open Project of State Key Laboratory of Supramolecular Structure and Materials (SKLSSM201407) and Open Project of State Key Laboratory of Theoretical and Computational Chemistry (K2013-02).

Notes and references

[a] *State Key Laboratory of Supramolecular Structure and Materials, College of Chemistry, Jilin University, Changchun 130012, P. R. China Tel: + 86-431-88499179, E-mail: luran@mail.jlu.edu.cn*

† Electronic Supplementary Information (ESI) available: UV-vis absorption and fluorescence spectra of **1-3** and **1B-3B**, ^{1}H and ^{13}C NMR spectra and mass spectrometry data for all new compounds, DFT caculation of configuration optimization materials and XRD pattern of xerogels. See DOI: 10.1039/b000000x/

1 (a) P. Terech and R. G. Weiss, *Chem. Rev.*, 1997, **97**, 3133-3159; (b) N. M. Sangeetha and U. Maitra, *Chem. Soc. Rev.*, 2005, **34**, 821-836; (c) R. G. Weiss, *J. Am. Chem. Soc.*, 2014, **136**, 7519-7530; (d) K. J. Skillig, F. Citossi, T. D. Bradshaw, M. Ashford, B. Kellam and M. Marlow, *Soft Matter*, 2014, **10**, 237-256; (e) J. W. Steed, *Chem. Comm.*, 2011, **47**, 1379-1383; (f) P. C. Xue, R. Lu, D. M. Li, M. Jin, C. H. Tan, C. Y. Bao, Z. M. Wang and Y. Y. Zhao, *Langmuir*, 2004, **20**, 11234-11239; (g) X. D. Yu, L. M. Chen, M. M. Zhang and T. Yi, *Chem. Soc. Rev*., 2014, **43**, 5346-5371; (h) Y. Feng, Y. M. He and Q. H. Fan, *Chem. Asian J*., 2014, **9**, 1724-1750; (i) T. Tu, W. W. Fang and Z. M. Sun, *Adv. Mater.*, 2013, **25**, 5304-5313.

2 (a) S. S. Babu, V. K. Praveen and A. Ajayaghosh, *Chem. Rev.*, 2014, **114**, 1973-2129; (b) A. Ajayaghosh, V. K. Praveen and C. Vijayakumar, *Chem. Soc. Rev*., 2008, **37**, 109-122; (c) F. J. M. Hoeben, P. Jonkheijm, E. W. Meijer and A. P. H. J. Schenning, *Chem. Rev*., 2005, **105**, 1491-1546; (d) Z. J. Zhao, J. W. Y. Lam and B. Z. Tang, *Soft Matter*, 2013, **9**, 4564-4579; (e) C. Wang, D. Q. Zhang and D. B. Zhu, *J. Am. Chem. Soc.*, 2005, **127**, 16372-16373.

3 (a) V. K. Praveen, C. Ranjith, E. Bandini, A. Ajayaghosh and N. Armaroli, *Chem. Soc. Rev.*, 2014, **43**, 4222-4242; (b) S. Bhattacharjee, S. Datta, S. Bhattacharya, *Chem. Eur. J*. **2013**, *19*, 16672-16681; (c) A. Ajayaghosh and V. K. Praveen, *Acc. Chem. Rev*., 2007, **40**, 644-656; (d) S. K. Samanta, A. Pal and S. Bhattacharya, *Lamgmuir*, **2009**, 25, 8567-8578; (e) C. Yao, Q. Lu, X. H. Wang and F. S. Wang, *J. Phys. Chem. B*, 2014, **118**, 4661-4668.

4 (a) Z. Q. Xie, V. Stepanenko, B. Fimmel and F. Würthner, *Mater. Horiz*., 2014, **1**, 355-359; (b)L. Xue, H. X. Wu, Y. Shi, H. Y. Liu, Y. L. Chen and X. Y. Li, *Soft Matter*, 2011, **7**, 6213-6221; (c) K. Sugiyasu, N. Fujita and S. Shinkai, *Angew. Chem. Int. Ed*., 2004, **43**, 1229-1233.

5 (a) B. K. An, J. Gierschner and S. Y. Park, *Acc. Chem. Res*., 2012, **45**, 544-554; (b) J. Lee, J. E. Kwon, Y. You and S. Y. Park, *Langmuir*, 2014, **30**, 2842-2851; (c)J. Seo, J. W. Chung, I. Cho and S. Y. Park, *Soft Matter*, 2012, **8**, 7617-7622; (d) C. D. Dou, D. Chen, J. Iqbal, Y. Yuan, H. Y. Zhang and Y. Wang, *Langmuir*, 2011, **27**, 6323-6329.

6 (a) L. Zhang, C. X. Liu, Q. X. Jin, X. F. Zhu and M. H. Liu, *Soft Matter*, 2013, **9**, 7966-7973; (b) X. F. Wang, P. F. Duan and M. H. Liu, *Chem. Asian J.*, 2014, **9**, 770-778; (c) X. D. Xu, J. Zhang, X. D. Yu, L. J. Chen, D. X. Wang, T. Yi, F. Y. Li and H. B. Yang, *Chem. Eur. J.*, 2012, **18**, 16000-16013; (d) K. Liu, T. H. Liu, X. L. Chen, X. H. Sun and Y. Fang, *ACS Appl. Mater. Interfaces*, 2013, **5**, 9830-9836; (e) N. Yan, Z. Y. Xu, K. K. Diehn, S. R. Raghavan, Y. Fang and R. G. Weiss, *J. Am. Chem. Soc*., 2013, **135**, 8989-8999.

7 (a) X. C. Yang, R. Lu, T. H. Xu, P. C. Xue, X. L. Liu and Y. Y. Zhao, *Chem. Commun.*, 2008, **4**, 453-455; (b) X. C. Yang, R. Lu, F. Y. Gai, P. C. Xue and Y. Zhan, *Chem. Commun.*, 2010, **46**, 1088-1090; (c) X. L. Liu, D. F. Xu, R. Lu, B. Li, C. Qian, P. C. Xue, X. F. Zhang and H. P. Zhou, *Chem. Eur. J*., 2011, **17**, 1660-1669; (d) X. L. Liu, X. F. Zhang, R. Lu, P. C. Xue, D. F. Xu and H. P. Zhou, *J. Mater. Chem*., 2011, **21**, 8756-8765; (e) P. C. Xue, B. Q. Yao, J. B. Sun, Z. Q. Zhang and R. Lu, *Chem. Common*., 2014, **50**, 10284-10286; (f) D. F. Xu, X. L. Liu, R. Lu, P. C. Xue, X. F. Zhang, H. P. Zhou and J. H. Jia, *Org. Biomol. Chem.*, 2011, **9**, 1523-1528; (g) C. Qian, K. Y. Cao, X. L. Liu, X. F. Zhang, D. F. Xu, P. C. Xue and R. Lu, *Chin. Sci. Bull*., 2012, **57**, 4264-4271; (h) G. H. Hong, C. Qian, P. C. Xue, X. L. Liu, Q. Q. Wang, M. Y. Liu, P. Gong and R. Lu, *Eur. J. Org. Chem.*, 2014, **28**, 6155-6162.

8 (a) P. A. Vigato, V. Peruzzo and S. Tamburini, *Coord. Chem. Rev*., 2009, **253**, 1099-1201; (b) J. Kido and Y. Okamoto, *Chem. Rev*., 2002, **102**, 2357-2368; (c) M. L. P. Reddy, V. Divya and R. Pavithran, *Dalton Trans*., 2013, **42**, 15249-15262; (d) D. M. Li, X. H. Tian, G. J. Hu, Q. Zhang, P. Wang, P. P. Sun, H. P. Zhou, X. M. Meng, J. X. Yang, J. Y. Wu, B. K. Jin, S. Y. Zhang, X. T. Tao and Y. P. Tian, *Inorg. Chem*., 2011, **50**, 7997-8006; (e) C. H. Chen, F. I. Wu, Y. Y. Tsai and C. H. Cheng, *Adv. Funct. Mater*., 2011, **21**, 3150-3158; (f) L. Carlucci, G. Ciani, S. Maggini, D. M. Proserpio and M. Visconti, *Chem. Eur. J*., 2010, **16**, 12328-12341.

9 (a) P. Galer, R. C. Korošec, M. Vidmar and B. Šket, *J. Am. Chem. Soc.*, 2014, **136**, 7383-7394; (b) G. Q. Zhang, J. B. Chen, S. J. Payne, S. E. Kooi, J. N. Demas and C. L. Fraser, *J. Am. Chem. Soc*., 2007, **129**, 8942-8943; (c) A. Felouat, A. D'Aléo and F. Fages, *J. Org Chem*., 2013, **78**, 4446-4455; (d)G. R. Kumar and P. Thilagar, *Dalton Trans*., 2014, **43**, 3871-3879; (e) B. Domercq, C. Grasso, J. L. Maldonado, M. Halik, S. Barlow, S. R. Marder and B. Kippelen, *J. Phys. Chem. B*, 2004, **108**, 8647-8651; (f)G. F. Bai, C. J. Yu, C. Cheng, E. H. Hao, Y. Wei, X. L. Mu and L. J. Jiao, *Org. Biomol. Chem*., 2014, **12**, 1618-1626.

10 (a) M. Halik, W. Wenseleers, C. Grasso, F. Stellacci, E. Zojer, S. Barlow, J. L. Brédas, J. W. Perry and S. R. Marder, *Chem. Comm.*, 2003**,** 1490-1491; (b) E. Cogné-Laage, J. F. Allemand, O. Ruel, J. Baudin, V. Croquette, M. Blanchard-Desce and L. Jullien, *Chem. Eur. J.*, 2004, **10**, 1445-1455; (c) J. M. Hales, S. J. Zheng, S. Barlow, S. R. Marder and J. W. Perry, *J. Am. Chem. Soc.*, 2006, **128**, 11362-11363.

11 (a) G. Q. Zhang, J. W. Lu, M. Sabat and C. L. Fraser, *J. Am. Chem. Soc*., 2010, **132**, 2160-2162; (b) X. X. Sun, X. P. Zhang, X. Y. Li, S. Y. Liu and G. Q. Zhang, *J. Mater. Chem.*, 2012, **22**, 17332-17339; (c) N. D. Nguyen, G. Q. Zhang, J. W. Lu, A. E. Sherman and C. L. Fraser, *J. Mater. Chem*., 2011, **21**, 8409-8415; (d) T. D. Liu, A. D. Chien, J. W. Lu, G. Q. Zhang and C. L. Fraser, *J. Mater. Chem*., 2011, **21**, 8401-8408; (e) G. Q. Zhang, J. P. Singer, S. E. Kooi, R. E. Evans, E. L. Thomas and C. L. Fraser, *J. Mater. Chem*., 2011, **21**, 8295-8299; (f) G. R. Krishna, M. S. R. N. Kiran, C. L. Fraser, U. Ramamurty and C. M. Reddy, *Adv. Funct. Mater.*, 2013, **23**, 1422-1430.

12 (a) C. T. Poon, W. H. Lam, H. L.Wong and V. W. Yam, *J. Am. Chem. Soc*., 2010, **132**, 13992; (b) A. D'Aléo, D. Gachet, V. Heresanu, M. Giorgi and F. Fages, *Chem. Eur. J.*, 2012, **18**, 12764-12772; (c) C. Z. Ran, X. Y. Xu, S. B. Raymond, B. J. Ferrara, K. Neal, B. J. Bacskai, Z. Medarova and A. Moore, *J. Am. Chem. Soc*., 2009, **131**, 15257-15261.

13 S. Chambon, A. D'Aléo, C. Baffert, G. Wantz and F. Fages, *Chem. Commun.*, 2013, **49**, 3555-3557.

14 Y. M. Sun, D.Rohde, Y. Q. Liu, L. J. Wan, Y. Wang, W. P. Wu, C. G. Di, G. Yu and D. B. Zhu, *J. Mater. Chem.*, 2006, **16**, 4499-4503.

15 (a) H. Maeda, *Chem. Eur. J.* , 2008, **14**, 11274-11282; (b) H. Maeda, Y. Haketa and T. Nakanish, *J. Am. Chem. Soc*., 2007, **129**, 13661-13674.

16 (a) X. F. Zhang, R. Lu, J. H. Jia, X. L. Liu, P. C. Xue, D. F. Xu and H. P. Zhou, *Chem. Commun*., 2010, **46**, 8419-8421; (b) X. F. Zhang, X. L. Liu, R. Lu, H. J. Zhang and P. Gong, *J Mater Chem*., 2012, **22**, 1167-1172.

17 J. Weng, Q. B. Mei, Q. L. Fan, Q. D. Ling, B. H. Tong and W. Huang, *RSC Adv*., 2013, **3**, 21877-21887.

18 C. H. Tan, L. H. Su, R. Lu, P. C. Xue, C. Y. Bao, X. L. Liu and Y. Y. Zhao, *J. Mol. Liq.*, 2006, **124**, 32-36.

19 K. Tanka, K. Tamashima, A. Nagai, T. Okawa and Y. Chujo, *Macromolecules*, 2013, **46**, 2969-2975.

20 C. Qian, G. H. Hong, M. Y. Liu, P. C. Xue and R. Lu, *Tetrahedron*, 2014, **70**, 3935-3942.

21 Gaussian 09, Revision A.02, M. J. Frisch, G. W. Trucks, H. B. Schlegel, G. E. Scuseria, M. A. Robb, J. R. Cheeseman, G. Scalmani, V. Barone, B. Mennucci, G. A. Petersson, H. Nakatsuji, M. Caricato, X. Li, H. P. Hratchian, A. F. Izmaylov, J. Bloino, G. Zheng, J. L. Sonnenberg, M. Hada, M. Ehara, K. Toyota, R. Fukuda, J. Hasegawa, M. Ishida, T. Nakajima, Y. Honda, O. Kitao, H. Nakai, T. Vreven, J. A. Montgomery, Jr., J. E. Peralta, F. Ogliaro, M. Bearpark, J. J. Heyd, E. Brothers, K. N. Kudin, V. N. Staroverov, R. Kobayashi, J. Normand, K. Raghavachari, A. Rendell, J. C. Burant, S. S. Iyengar, J. Tomasi, M. Cossi, N. Rega, J. M. Millam, M. Klene, J. E. Knox, J. B. Cross, V. Bakken, C. Adamo, J. Jaramillo, R. Gomperts, R. E. Stratmann, O. Yazyev, A. J. Austin, R. Cammi, C. Pomelli, J. W. Ochterski, R. L. Martin, K. Morokuma, V. G. Zakrzewski, G. A. Voth, P. Salvador, J. J. Dannenberg, S. Dapprich, A. D. Daniels, Ö. Farkas, J. B. Foresman, J. V. Ortiz, J. Cioslowski and D. J. Fox, Gaussian, Inc., Wallingford CT, 2009.

22 Y. Zhan, K. Y. Cao, C. G. Wang, J. H. Jia, P. C. Xue, X. L. Liu, X. M. Duan and R. Lu, *Org. Biomol. Chem.*, 2012, **10**, 8701-8709.

23 (a) W. W. Zhang, W. L. Mao, Y. X. Hu, Z. Q. Tian, Z. L. Wang and Q. J. Meng, *J. Phys. Chem. A*, 2009, **113**, 9997-10004; (b) J. H. Jia, K. Y. Cao, P. C. Xue, Y. Zhang, H. P. Zhou and R. Lu, *Tetrahedron*, 2012, **68**, 3626-3632; (c) J. H. Jia, Y. Zhang, P. C. Xue, P. Zhang, X. Zhao, B. J. Liu and R. Lu, *Dyes Pigments*, 2013, **96**, 407-413.

24 (a) D. Li, H. Y. Zhang, C. G. Wang, S. Huang, J. H. Gao and Y, Wang, *J. Mater. Chem.*, 2012, **22**, 4319-4328; (b) M. Shimizu, Y. Takeda, M. Higashi and T. Hiyama, *Angew. Chem. Int. Ed.*, 2009, **48**, 3653-3656.

25 T. Khanasa, N. Prachumrak, R. Rattanawan, S. Jungsuttiwong, T. Keawin, T. Sudyoadsuk, T. Tuntulani and V. Promarak, *Chem. Commun*., 2013, **49**, 3401-3403.

26 P. Gong, P. C. Xue, C. Qian, Z. Q. Zhang and R. Lu, *Org. Biomol. Chem*., 2014, **12**, 6134-6144.

27 (a) C. Y. Bao, R. Lu, M. Jin, P. C. Xue, C. H. Tan, T. H. Xu, G. F. Liu and Y. Y. Zhao, *Chem. Eur. J*., 2006, **12**, 3287-3294; (b) O. Simalou, R. Lu, P. C. Xue, P. Gong and T. R. Zhang, *Eur. J. Org. Chem*., 2014, **14**, 2907-2916; (c) O. Simalou, P. C. Xue and R. Lu, *Tetrahedron Lett*., 2010, **51**, 3685-3690.

28 (a) Z. Chen, V. Stepaninko, V. Dehm, P. Prins, L. D. A. Siebbeles, J. Seibt, P. Marquetand, V. Engel and F. Würthner, *Chem. Eur. J.*, 2007, **13**. 436-449; (b) F. Würthner, *Chem. Commun*., 2004, 1564-1579.

29 a) Y. Hong, J. W. Y. Lam, B. Z. Tang, *Chem. Soc. Rev.* **2011**, 40, 5361-5388; b) S. Datta, and S. Bhattacharya, *Chem. Commun.* **2012**, 48, 877-879.

30 X. C. Yang, R. Lu, H. P. Zhou, P. C. Xue, F. Y. Wang, P. Chen and Y. Y. Zhao, *J. Colloid. Interf. Sci.*, 2009, **339**, 527-532.

31 Y. Feng, Z. T. Liu, J. Liu, Y. M. He, Q. Y. Zheng and Q. H. Fan, *J. Am. Chem. Soc*., 2009, **131**, 7950-7951.

32 (a) P. C. Xue, R. Lu, G. J. Chen, Y. Zhang, H. Nomoto, M. Takafuji and H. Ihara, *Chem. Eur. J.*, 2007, **13**, 8231-8239; (b) P. Chen, R. Lu, P. C. Xue, T. H. Xu, G. J. Chen and Y. Y. Zhao, *Langmuir*, 2009, **25**, 8395-8399.

33 (a) A. P. Sivadas, N. S. S. Kumar, D. D, Prabhu, S. Varghese, S. K. Prasad, D. S. S. Rao and S. Das, *J. Am. Chem. Soc.*, 2014, **136**, 5416-5423; (b) H. Maeda, Y. Terashima, Y. Haketa, A. Asano, Y. Honsho, S. Seki, M. Shimizu, H. Mukai and K. Ohta, *Chem. Commun.*, 2010, **46**, 4559-4561.